Available online at www.sciencedirect.com
ScienceDirect
Dyes and Pigments 75 (2007) 328–334
DYES and PIGMENTS
www.elsevier.com/locate/dyepig

Ultra-fine particles formation of C.I. Pigment Green 36 in different phase regions via a supercritical anti-solvent process

Hsien-Tsung Wu, Ho-Mu Lin, Ming-Jer Lee*

Department of Chemical Engineering, National Taiwan University of Science and Technology, 43 Keelung Road, Section 4, Taipei 106-07, Taiwan

Received 22 May 2006; accepted 8 June 2006
Available online 2 August 2006

Abstract

Ultra-fine particles of C.I. Pigment Green 36 were prepared using a continuous supercritical anti-solvent (SAS) apparatus employing quinoline as solvent and supercritical carbon dioxide as anti-solvent. A series of precipitation experiments were conducted at different temperatures, pressures, and flow rates of pigment solution. The vapor–liquid phase boundaries of carbon dioxide + quinoline mixtures were also measured with a volume-variable phase equilibrium analyzer at temperatures from 308.2 K to 328.2 K. Mapping the estimated composition of mixtures in a model CSTR (continuously stirred tank reactor) precipitator at the end of injection of pigment solution onto the phase diagram found that the morphology of prepared particles was mainly governed by the phase behavior of anti-solvent + solvent mixtures. Nano-particles were obtained as the precipitation loci were manipulated within either supercritical or superheated vapor region through the SAS process, whereas micro-metric aggregated ball-like particles were produced as the precipitation loci passed by the vapor–liquid coexistence region.

Keywords: Supercritical carbon dioxide; Anti-solvent; Nano-particles; Pigment Green 36

1. Introduction

Nano-metric or submicron pigment particles are essential materials for use in photo resists, which are used for fabricating color filters and for color liquid crystal displays (color-LCD). The smaller sizes of pigment particles in the dispersion media yield superior color strength, contrast, and transmittance [1]. Therefore, searching for feasible methods and favorable process parameters to produce nano-metric pigment particles with narrow particle size distribution (PSD) is technically important for the industrial applications. Instead of traditional mechanical milling, the supercritical anti-solvent (SAS) process may provide an innovative route to meet this demand [1–3]. Previous studies on pigment particle formation using supercritical techniques are rather limited. Gao et al. [4] prepared micro-metric particles of Pigment Red Lake C, C.I. Pigment Yellow 1, and C.I. Pigment Blue 15 using an SAS method. Micro-metric pigment particles of Bronze Red were produced by Hong et al. [5] with a continuous SAS apparatus. Wu et al. [1,6] extensively investigated the effects of the SAS process parameters on the PSD of C.I. Pigment Red 177 and C.I. Pigment Blue 15:6. Nano-metric or submicron particles were obtained from these studies. The precipitation kinetic parameters of Pigment Blue 15:6 were determined with the aid of the population balance theory [6]. Reverchon et al. [7] investigated micronization of C.I. Disperse red 60 using both SAS and supercritical-assisted atomization (SAA) methods. They found that nano-metric particles could be formed using SAS, whereas micro-metric particles were produced using SAA. Wu et al. [8] developed a supercritical-assisted dispersion apparatus to C.I. Pigment Red 177 in propylene glycol monomethyl ether acetate with blended dispersants.

In addition to Wubbolts et al. [9] and Wu et al. [1,6], Reverchon et al. [10] found that the phase behavior of mixtures in precipitator, rather than the mass transfer, governed SAS precipitation. As shown from their experimental results,

* Corresponding author. Tel.: +886 2 2737 6626; fax: +886 2 2737 6644.
E-mail address: mjl@ch.ntust.edu.tw (M.-J. Lee).

0143-7208/$ - see front matter © 2006 Elsevier Ltd. All rights reserved.
doi:10.1016/j.dyepig.2006.06.006

submicron particles were produced when the mixtures of solvent + anti-solvent + solute in the precipitator were manipulated at supercritical homogeneous states during the particle formation stage. Micro-metric powders, however, were obtained as the precipitation was conducted in the vapor–liquid coexistence region. The vapor–liquid equilibrium (VLE) data of anti-solvent + solvent mixtures thus provide valuable information for particle design using the SAS method.

C.I. Pigment Green 36 is widely used in preparing photo resists. Nano-particles of this pigment were produced, in the present study, using a continuous SAS apparatus employing quinoline as solvent and supercritical carbon dioxide as anti-solvent. The experiments were conducted at various flow rates of pigment solutions over the temperature range 308.2–328.2 K and pressures of up to 31 MPa. The collected particles samples were analyzed using field emission scanning electron microscopy (FESEM) and the PSD and the mean sizes of particles were then determined with an image processing software. Since the phase behavior played an important role in the SAS precipitation, the vapor–liquid phase boundaries (bubble and dew points), including near critical region, were also measured in this study with the volume-variable phase equilibrium analyzer for carbon dioxide + quinoline at 308.2 K, 318.2 K, and 328.2 K over a wide range of pressures. The composition variations of fluid mixtures in the precipitator during the courses of injection and purge stages were estimated from a simple continuously stirred tank reactor (CSTR) model, and the calculated precipitation loci were mapped onto the phase diagram of carbon dioxide + quinoline to examine the influence of the phase behavior on the resultant pigment particles.

2. Experimental section

2.1. Materials

C.I. Pigment Green 36 (Cu-phthalocyanine, halogenated) was supplied by Ciba Special Chemicals Co., Hong Kong. Its chemical structure is shown in Fig. 1. The particle sizes of the pigment as received distribute in the range of 1–20 μm. Quinoline (purity of 99.9%, spectrophotometric grade) was purchased from Aldrich (USA) and carbon dioxide (purity of 99.8%) from Liu-Hsiang Gas Co., Taiwan. These chemicals were used without further purification.

2.2. Apparatus and operation

A volume-variable phase equilibrium analyzer was utilized to investigate the phase boundary (bubble and dew points) of the binary mixtures of carbon dioxide + quinoline. The apparatus and the experimental procedure have been detailed elsewhere [1]. The uncertainties of measurements are ±0.1 K, ±0.05 Mpa, and ±0.003 for temperature, pressure, and composition in mole fraction, respectively.

The schematic diagram of the continuous SAS apparatus and the operation procedure of the experiment have also been reported by Wu et al. [1]. An HPLC pump was used for delivery of pigment solution and another high-pressure liquid pump for carbon dioxide. These two pressurized streams were pre-heated in a thermostatic air bath, and then diverted into the precipitator, from the top, through a coaxial injection tube. The coaxial injector consisted of a 0.3175 cm (outside diameter) stainless steel tube with an insert of PEEK capillary tube (63 μm, inside diameter). The pigment solution was injected into the precipitator via the capillary tube and carbon dioxide was delivered via the stainless steel tube (outside the capillary tube). The precipitation chamber was made of stainless steel with an internal volume of 49 cm^3. A metal frit was mounted at the outlet (bottom) of the precipitator to retain the produced pigment particles. Four glass-plates were placed in the precipitator at different positions to collect the particulate samples. The pre-heaters, the coaxial injector, and the precipitator were placed in the thermostatic air bath, which was controlled to within ±0.1 K. The bath temperature was measured by a precision platinum RTD sensor to an uncertainty of ±0.02 K. A pressure transducer with a digital indicator measured the operating pressure in the precipitator, accurate to ±0.1%. A separator followed the precipitator to separate solvent and anti-solvent at near atmospheric pressure. The flow rate and the total volume of carbon dioxide passing through the precipitator were determined with a wet test meter to an uncertainty of ±0.25%. The mass flow rate of carbon dioxide was manipulated at about 0.03 g/s through the precipitation stage in each run. The total volume of the injected pigment solutions was about 8 cm^3. After the precipitation stage, carbon dioxide was kept continuously charging into the precipitator for about 150 min in order to remove the residual solvent in the chamber. At least 300 particles on an FESEM image were counted for determining the PSD and the mean particle size by using the software of the Sigma Scan Pro5. All precipitation runs were conducted twice at each experimental condition. The mean particle size of the replicated samples was reproducible to within about ±3 nm.

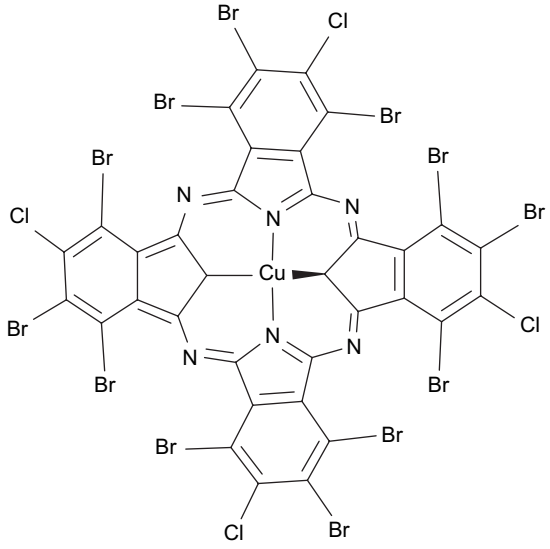

Fig. 1. Chemical structure of Pigment Green 36.

3. Results and discussion

3.1. Vapor–liquid equilibrium phase diagram of anti-solvent + solvent system

The phase behavior of the fluid mixtures in a precipitator has been recognized as one of crucial factors to control the particle formation with the SAS process. Due to the extremely minute solubility of C.I. Pigment Green 36 in supercritical carbon dioxide, the phase behavior of the mixtures in the precipitator should be very similar to that of the mixtures without containing the pigment, i.e., the binary mixtures of carbon dioxide + quinoline [6]. The vapor–liquid phase boundaries (including dew points and bubble points) of the binary system of carbon dioxide + quinoline were thus measured with the volume-variable phase equilibrium analyzer over a temperature range of 308.2–328.2 K and up to critical pressures. Fig. 2 illustrates the experimental results in which x_{CO_2} stands for the mole fraction of carbon dioxide. This phase diagram is divided into four phase regions, including vapor–liquid coexistence (V–L), compressed liquid (L), superheated vapor (V), and supercritical (SC) regions. The critical pressure and composition at each temperature were estimated from the maximum point of the smoothed isothermal phase boundary near the critical region. The estimated critical points are located at 308.2 K/23.9 MPa/x_{CO_2} = 0.843, 318.2 K/25.3 MPa/x_{CO_2} = 0.842, 328.2 K/26.9 MPa/x_{CO_2} = 0.842.

3.2. Influence of phase behavior on morphology of resultant particles

The precipitation experiments were conducted at different volumetric flow rates of pigment solution (F, from 0.0100 cm^3/s to 0.0667 cm^3/s), precipitation temperatures (T, from 308.2 K to 328.2 K), and precipitation pressures (P, from 20 MPa to 31 MPa), but the concentration of the injected pigment solution was fixed at 0.08 kg/m^3 through all the experimental runs due to the low solubility of Pigment Green 36 in quinoline. The experimental conditions and the results are reported in Table 1, where the densities of carbon dioxide at precipitation temperature and pressure were taken from the NIST Chemistry WebBook [11].

The composition variations of fluid mixtures in the precipitation chamber during the SAS process were calculated, in this study, from unsteady-state material balance equations around the precipitator. The estimated results can be mapped onto the phase diagram of carbon dioxide + quinoline to identify the phase regions being passed during the SAS procedure. Similar to the work of Schmitt et al. [12], the precipitator was assumed as a continuously stirred tank reactor (CSTR) with two inlet and one outlet streams. With the initial condition of pure carbon dioxide (z_{CO_2} = 1.0, where z_{CO_2} is the mass fraction of carbon dioxide) at the beginning of injection of pigment solution ($t = 0$), the analytical solution of z_{CO_2} varying with time (t) is given as follows [12]:

$$z_{CO_2} = \left(\frac{M_{CO_2}}{M_{CO_2} + x_S \rho F}\right) + \left(\frac{x_S \rho F}{M_{CO_2} + x_S \rho F}\right) \exp\left[\frac{-(M_{CO_2} + x_S \rho F)t}{M_f^{sys}}\right] \quad (1)$$

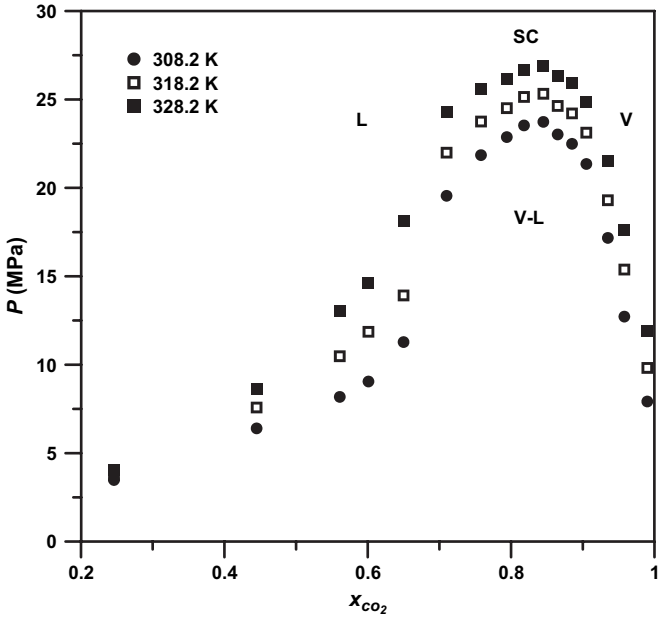

Fig. 2. VLE phase diagram of carbon dioxide + quinoline system.

Table 1
Experimental conditions and results

Run	C (kg/m^3)	P (Mpa)	T (K)	F (cm^3/s)	ρ_{CO_2} (g/cm^3)[a]	Mean size (nm)	σ (nm)[b]
1	0.08	25	308.2	0.0167	0.902	44.5	6.5
2[c]	0.08	23	308.2	0.0167	0.889	48.6	9.4
3	0.08	27	308.2	0.0167	0.913	45.2	6.2
4	0.08	28	308.2	0.0167	0.919	45.5	6.3
5	0.08	29	308.2	0.0167	0.924	40.0	5.4
6	0.08	31	308.2	0.0167	0.934	45.1	7.0
7	0.08	25	313.2	0.0167	0.879	49.0	6.9
8[c]	0.08	25	318.2	0.0167	0.857	47.6	7.1
9[c]	0.08	25	328.2	0.0167	0.811	50.8	6.6
10	0.08	25	308.2	0.0100	0.902	45.9	7.3
11	0.08	25	308.2	0.0250	0.902	42.7	6.5
12	0.08	25	308.2	0.0500	0.902	44.5	7.8
13	0.08	25	308.2	0.0667	0.902	45.7	7.5
14[c]	0.08	23	318.2	0.0167	0.841	49.5	8.9
15	0.08	28	318.2	0.0167	0.878	49.7	7.0
16	0.08	28	328.2	0.0333	0.836	51.9	7.0
17[d]	0.08	20	308.2	0.0500	0.866	–	–
18[d]	0.08	20	318.2	0.0500	0.813	–	–
19[d]	0.08	20	328.2	0.0500	0.755	–	–
20[d]	0.08	23	328.2	0.0167	0.791	–	–

[a] Density of carbon dioxide at precipitation temperature and pressure. The values were taken from the NIST Chemical WebBook [11].
[b] Standard deviation.
[c] Operated in superheated vapor region. Precipitations were conducted in supercritical region if not indicated.
[d] Passed by vapor–liquid coexistence region.

where M_{CO_2} (g/s) is the mass flow rate of the inlet carbon dioxide, x_S is the mass fraction of solvent (quinoline) in the injected pigment solution ($x_S = 1.0$), ρ is the density of pigment solution (about 1.090 g/cm^3), F (cm^3/s) is the volumetric flow rate of the injected pigment solution, and M_f^{sys} (g) is the total mass of fluid phase in the precipitator which was assumed to be remained a constant with time and was approximated by the mass of pure carbon dioxide in the whole precipitator at the beginning of injection of pigment solution.

Upon ending injection (at $t = t^0$), a purge (or drying) operation was followed by continuously charging the pure carbon dioxide into the precipitator. The variation of the mass fraction of carbon dioxide (z'_{CO_2}) during this purge stage was also derived by Schmitt et al. [12] as follows:

$$z' = 1 + \left(z^0_{CO_2} - 1\right)\exp\left[\frac{-(M_{CO_2})(t - t^0)}{M_f^{sys}}\right] \quad (2)$$

where $z^0_{CO_2}$ is the mass fraction of carbon dioxide at the end of injection ($t = t^0$). The detailed derivation for Eqs. (1) and (2) has been given by Schmitt et al. [12]. The mass fraction z_{CO_2} can be readily converted into mole fraction x_{CO_2} by

$$x_{CO_2} = \frac{z_{CO_2}/44.01}{(z_{CO_2}/44.01) + (1 - z_{CO_2})/129.262} \quad (3)$$

Fig. 3 is an illustrative example of the calculated mole fraction of carbon dioxide x_{CO_2} in the precipitator varying with time, including injection and purge stages. The horizontal lines on the graph represent the vapor–liquid phase boundaries, i.e., the composition of the dew point at the corresponding precipitation conditions. The mole fraction of carbon dioxide decreases from unity to a minimum value ($x^0_{CO_2}$) at the end of injection of pigment solution. After that, x'_{CO_2} increases with an increase of time and approaches to unity when the residual solvent in the precipitator was totally removed. As seen from the graph, the locus of run #9 is well above the horizontal solid line through the injection and purge stages. However, the locus of run #19 crosses the horizontal dashed line twice. It means that the fluid mixtures in the precipitator had passed by the vapor–liquid coexistence region during the SAS process. While the mixing in precipitator was non-ideal, the actual minimum concentration of carbon dioxide $x^0_{CO_2}$ should be lower than the value calculated from Eq. (1).

The estimated minimum concentrations of carbon dioxide $x^0_{CO_2}$, at the end of injection of pigment solution, were marked on Figs. 4–6 for the experiments conducted at 308.2 K, 318.2 K and 328.2 K, respectively. The horizontal dashed line stands for the critical pressure at the precipitation temperature and the solid curve for the vapor–liquid phase boundary. The particle formation occurred in the supercritical region, if the points are above the horizontal dashed line, such as runs #1, #3–#6, #10–#13 (in Fig. 4), run #15 (in Fig. 5), and run #16 (in Fig. 6). The precipitation and purge stages were operated in the superheated vapor regions, if the points are located under the horizontal dashed line but well behind the right hand side of the vapor–liquid phase boundaries, such as run #2 (in Fig. 4), runs #8 and #14 (in Fig. 5), and run #9 (in Fig. 6). In the case of the points located on the left hand side or near the phase boundaries, such as run #17 (in Fig. 4), run #18 (in Fig. 5), and runs #19 and #20 (in Fig. 6), the SAS procedure was likely to crossing the vapor–liquid coexistence region. Although the estimated minimum compositions of carbon dioxide of runs #17 and #20 are located in the superheated vapor region, actually these

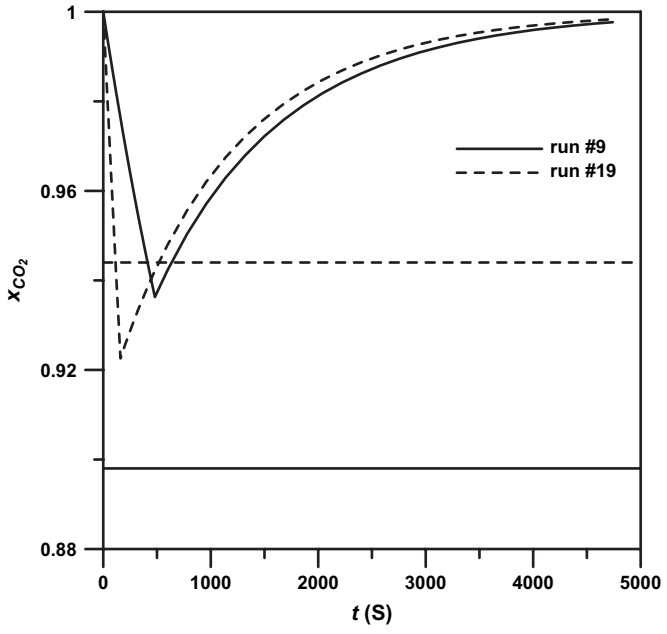

Fig. 3. Mole fractions of carbon dioxide in precipitator varying with time during the SAS process.

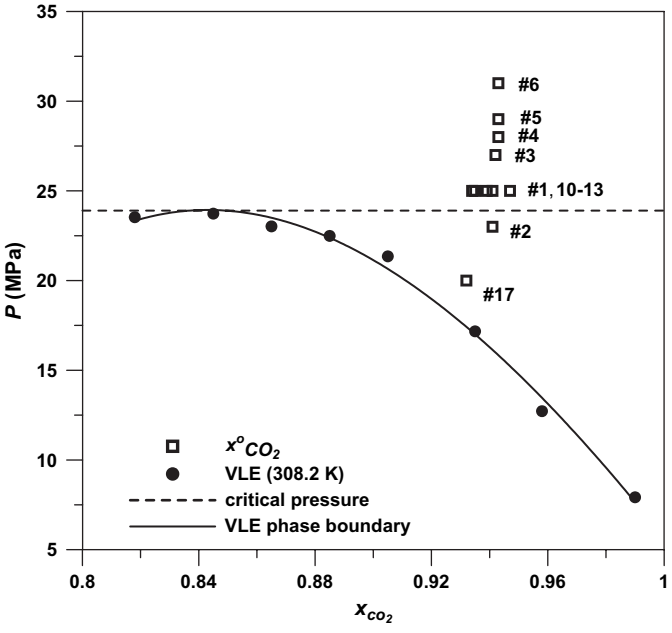

Fig. 4. VLE phase boundary and the estimated compositions of carbon dioxide in precipitator at the end of injection of pigment solution for the experimental runs at 308.2 K.

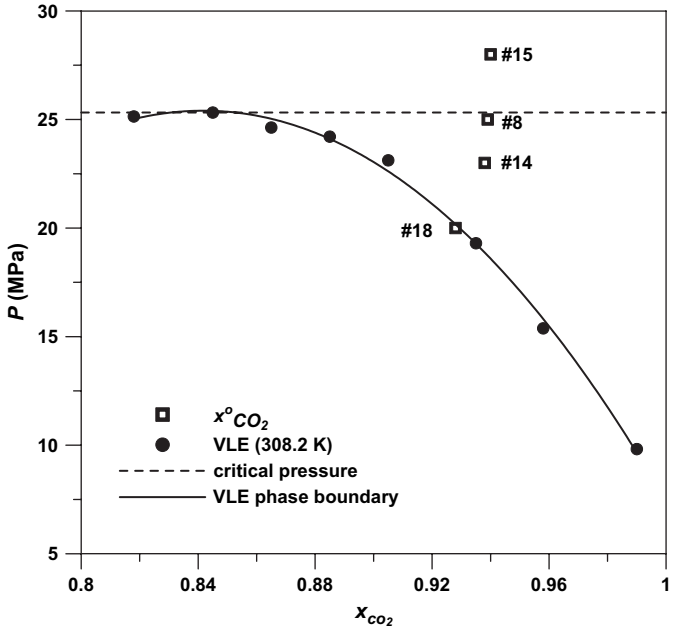

Fig. 5. VLE phase boundary and the estimated compositions of carbon dioxide in precipitator at the end of injection of pigment solution for the experimental runs at 318.2 K.

runs should pass by the two-phase coexistence region at the end of injection of pigment solution because the recovered quinoline from the separator was found to turn into greenish. As noted earlier, this discrepancy may be attributed to the non-ideal mixing in the precipitator.

Fig. 7 shows the FESEM images of the samples prepared in the vapor–liquid coexistence region (run #18, Fig. 7(a)), in the supercritical region (run #10, Fig. 7(b)), and in superheated vapor region (run #14, Fig. 7(c)), respectively. Fig. 8 is the corresponding enlarged FESEM images. As seen from the images, the shape of the resultant primary particles of Pigment Green 36 is nearly spherical. The images also illustrate that micro-metric aggregated ball-like particles were formed

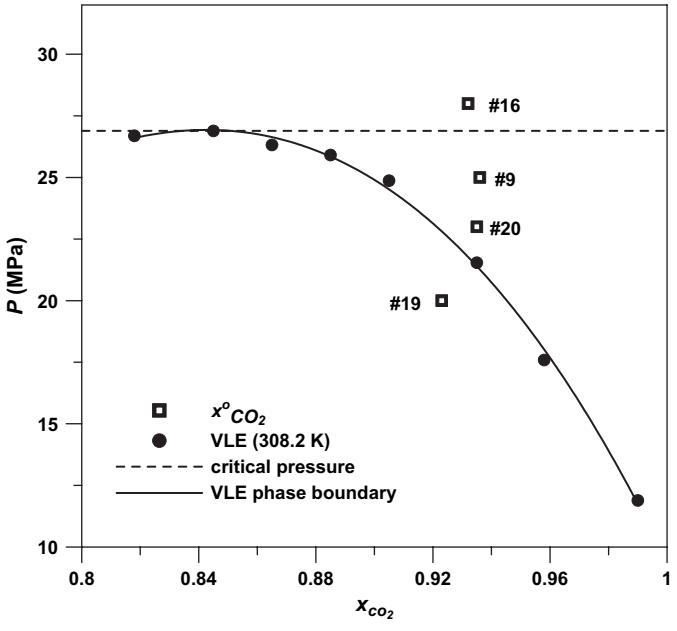

Fig. 6. VLE phase boundary and the estimated compositions of carbon dioxide in precipitator at the end of injection of pigment solution for the experimental runs at 328.2 K.

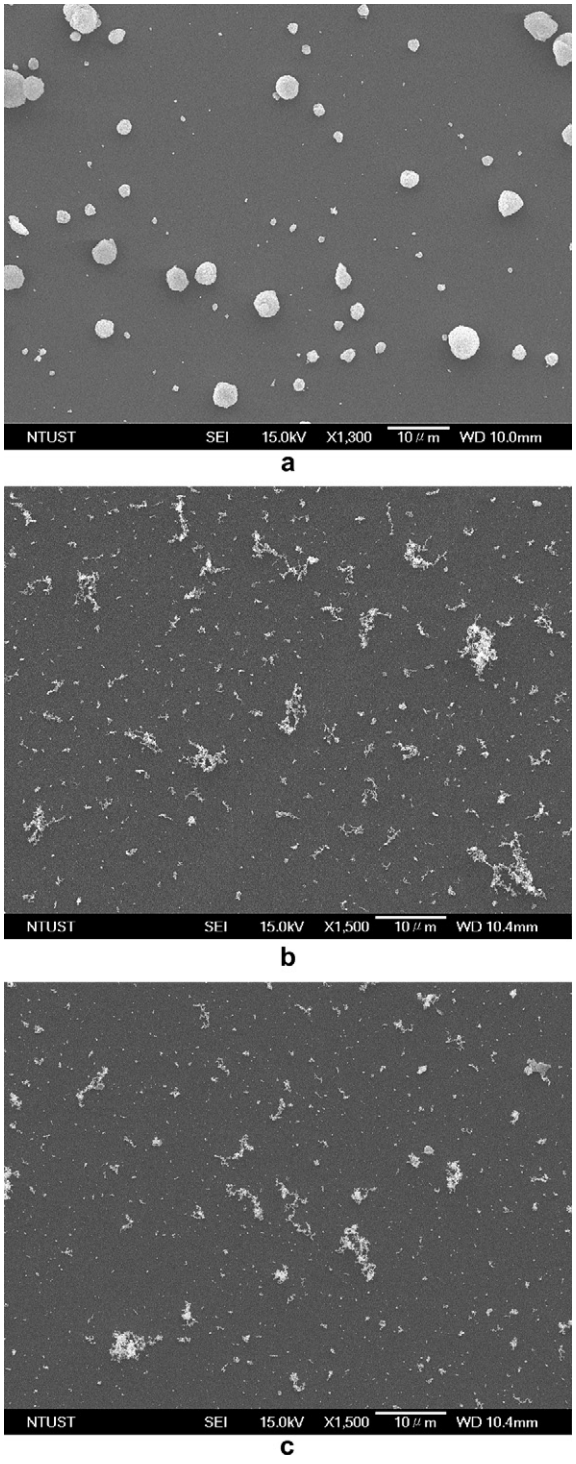

Fig. 7. FESEM images of the samples taken from the experiment of (a) run #18, at $T = 318.2$ K, $P = 20$ MPa, $F = 0.05$ cm^3/s, crossing the vapor–liquid coexistence region; (b) run #10, at $T = 308.2$ K, $P = 25$ MPa, $F = 0.01$ cm^3/s, in supercritical region; (c) run #14, at $T = 318.2$ K, $P = 23$ MPa, $F = 0.0167$ cm^3/s, in superheated vapor region.

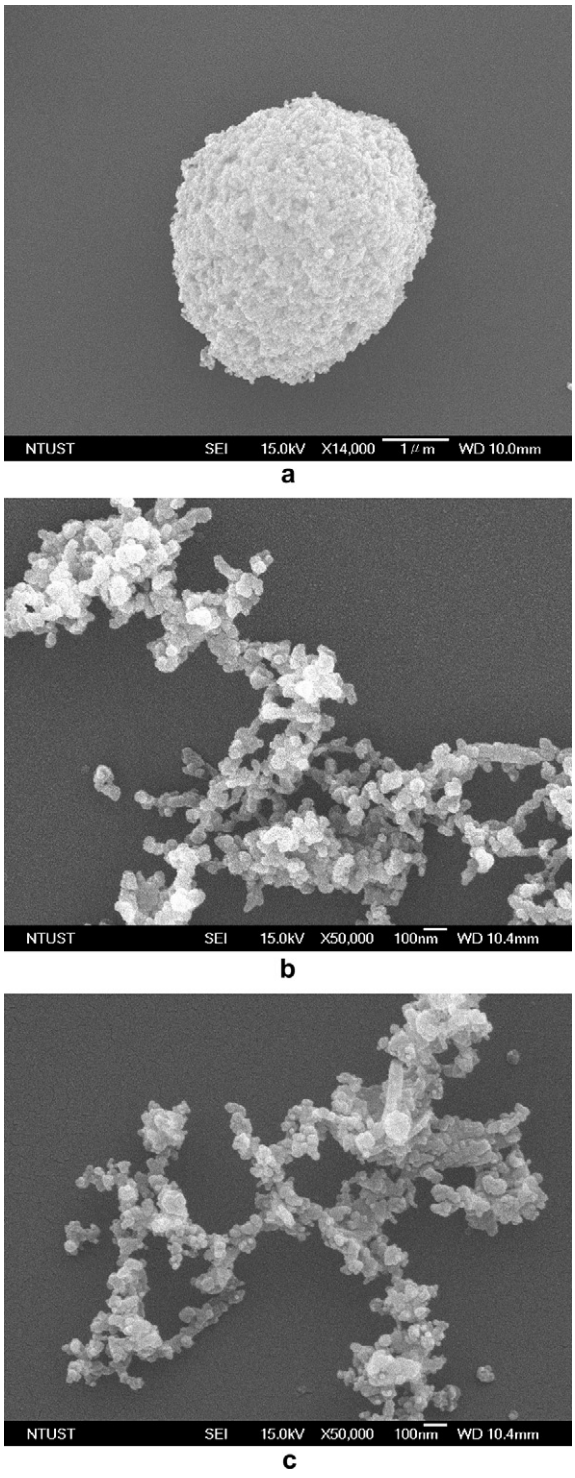

Fig. 8. The corresponding enlarged FESEM images of Fig. 7(a)–(c).

when the SAS process passed by the vapor–liquid coexistence region. Nano-metric and less aggregated pigment particles were produced when the SAS process was operated in either supercritical or superheated vapor region. In the former case serious aggregations were suggested to occur in the existing liquid phase, whereas in the latter cases the particles were formed in ''dry'' environments.

3.3. Influences of process parameters on particle size

Fig. 9(a)–(c) presents the mean particle size varying with flow rate of pigment solution (F), precipitation pressure (P), and precipitation temperature (T), respectively. These graphs show that the differences of mean particle sizes among all the resultant pigment products are almost within the experimental uncertainty (±3 nm) over the entire range of the individual process parameters, and the mean sizes of the majority cases are in the range of 40–50 nm. Additionally, the dependences of resultant particle sizes on both temperature and pressure can also be represented as a function of density. In the precipitation experiments, carbon dioxide is a predominant component in the fluid mixtures, and thus the mixture density should be very close to the density of pure carbon dioxide. Fig. 10 depicts the mean particle size varying with the density of carbon dioxide for those experiments operated in either

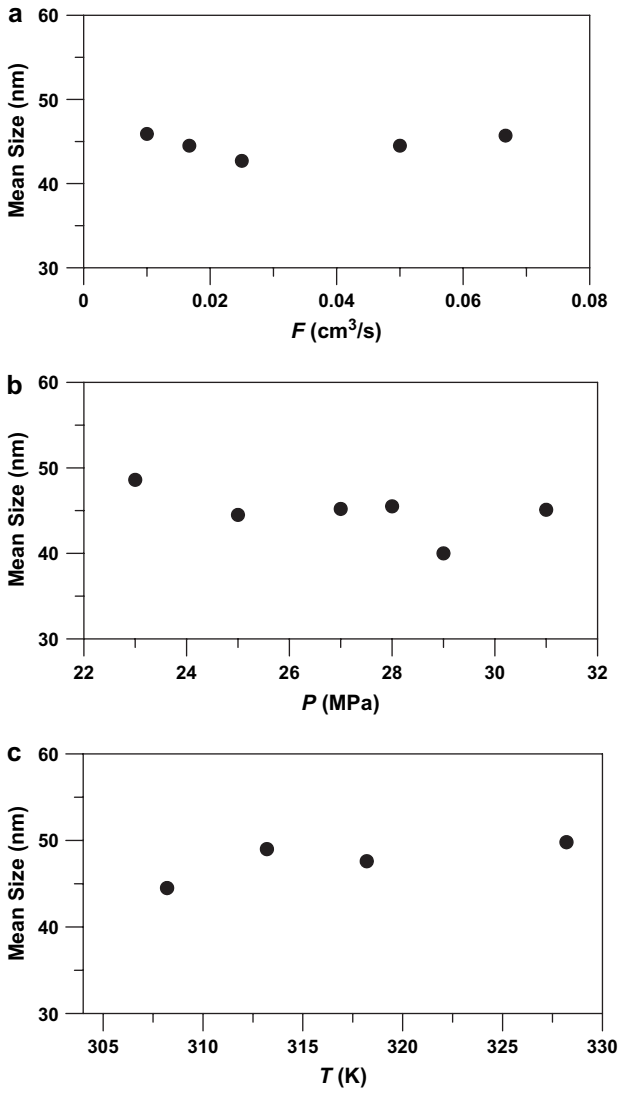

Fig. 9. Mean particle size varying with the process parameter of: (a) flow rate of pigment solution, at $P = 25$ MPa and $T = 308.2$ K; (b) pressure, at $T = 308.2$ K and $F = 0.0167$ cm^3/s; (c) temperature, at $P = 25$ MPa and $F = 0.0167$ cm^3/s.

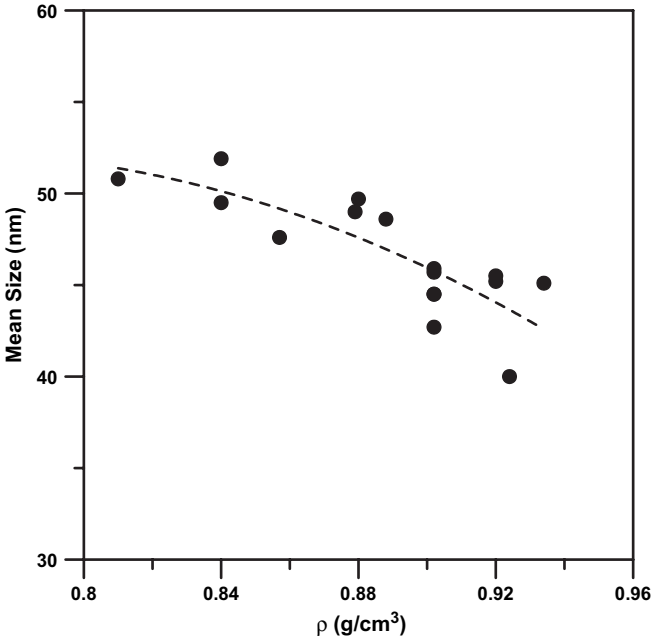

Fig. 10. Mean particle size varying with density of carbon dioxide at the precipitation conditions.

supercritical or superheated region (runs #1–#16). In these two homogeneous phase regions, a qualitative trend was found such that higher densities of the fluid mixtures in the precipitator are favorable to reduce the mean size of resultant pigment particles. Nevertheless, nano-metric pigment particles of Green 36 can be produced over a wide range of operating conditions, only if the precipitation is conducted in a homogeneous phase region, either at supercritical or at superheated vapor states. When the precipitation pressures are lower than the corresponding critical value, the relative flow rates between of carbon dioxide and the pigment solution should be sufficiently large to ensure that the precipitation was made in the superheated vapor region.

4. Conclusions

Nano-particles of C.I. Pigment Green 36 were successfully prepared with a continuous supercritical anti-solvent (SAS) apparatus using quinoline as a solvent and supercritical carbon dioxide as anti-solvent. The morphology of the resultant products closely depends on the phase regions where precipitation was implemented. Micro-metric aggregated ball-like particles were produced via the SAS process passed by the vapor–liquid coexistence region, whereas nano-metric particles, ranging from 40 nm to 50 nm, were obtained in both the supercritical and superheated vapor region. The concentration of the fluid mixtures in the precipitator during the SAS process can be estimated by a simple CSTR model. The vapor–liquid equilibrium phase diagram together with this CSTR model provides valuable information for manipulating the particulate products. The experimental results also showed that higher densities of fluid mixtures in the precipitator may be favorable to reduce the particle size of the resultant products.

Acknowledgements

The authors gratefully acknowledge the financial support of the National Science Council, Taiwan, through Grant No. NSC-94-2214-E011-009. The authors also thank Mr. H.Y. Chiu for the measurements of phase boundaries and Dr. J.T. Chen, Department of Chemical Engineering, Ming Hsin University of Science and Technology, for valuable discussion.

References

[1] Wu HT, Lee MJ, Lin HM. Nano-particles formation for pigment red 177 via a continuous supercritical anti-solvent process. J Supercrit Fluids 2005;33:173.
[2] Reverchon E. Supercritical antisolvent precipitation of micro- and nanoparticles. J Supercrit Fluids 1999;15:1.
[3] Jung J, Perrut M. Particle design using supercritical fluids: literature and patent survey. J Supercrit Fluids 2001;20:179.
[4] Gao Y, Mulenda TK, Shi YF, Yuan WK. Fine particles preparation of red lake C pigment by supercritical fluid. J Supercrit Fluids 1998;13:369.
[5] Hong L, Guo JZ, Gao Y, Yuan WK. Precipitation of microparticulate organic powders by a supercritical antisolvent process. Ind Eng Chem Res 2000;39:4482.
[6] Wu HT, Lee MJ, Lin HM. Precipitation kinetics of pigment blue 15:6 sub-micro particles with a supercritical anti-solvent process. J Supercrit Fluids 2006;37:220.
[7] Reverchon E, Adami R, De Macro I, Laudani CG, Spada A. Pigment red 60 micronisation using supercritical fluids based techniques. J Supercrit Fluids 2005;35:76.
[8] Wu HT, Lee MJ, Lin HM. Supercritical fluid-assisted dispersion of ultrafine pigment red 177 particles with blended dispersants. J Supercrit Fluids, in press.
[9] Wubbolts FE, Bruinsma OSL, van Rosmalen GM. Dry-spraying of ascorbic acid or acetaminophen solutions with supercritical carbon dioxide. J Cryst Growth 1999;198/199:767.
[10] Reverchon E, Caputo G, De Marco I. Role of phase behavior and atomization in the supercritical antisolvent precipitation. Ind Eng Chem Res 2003;42:6406.
[11] Isothermal properties for carbon dioxide. NIST Chemistry WebBook, NIST Standard Reference Database No. 69 – March 2003, Release, <http://webbook.nist.gov/chemistry/>.
[12] Schmitt WJ, Salada MC, Shook GG, Speaker III SM. Finely-divided powders by carrier solution injection into a near or supercritical fluid. AIChE J 1995;41:2476.